Journal of Hazardous Materials 172 (2009) 338–344

Contents lists available at ScienceDirect

Journal of Hazardous Materials

journal homepage: www.elsevier.com/locate/jhazmat

Nanosized $BiVO_4$ with high visible-light-induced photocatalytic activity: Ultrasonic-assisted synthesis and protective effect of surfactant

Meng Shang, Wenzhong Wang*, Lin Zhou, Songmei Sun, Wenzong Yin

State Key Laboratory of High Performance Ceramics and Superfine Microstructures, Shanghai Institute of Ceramics, Chinese Academy of Sciences, 1295 DingXi Road, Shanghai 200050, PR China

ARTICLE INFO

Article history:
Received 17 February 2009
Received in revised form 11 June 2009
Accepted 4 July 2009
Available online 25 July 2009

Keywords:
Nanosize
$BiVO_4$
Ultrasonic
PEG
Visible-light photocatalysis

ABSTRACT

Nanosized $BiVO_4$ with high visible-light-induced photocatalytic activity was successfully synthesized via ultrasonic-assisted method with polyethylene glycol (PEG). The $BiVO_4$ sample prepared under ultrasonic irradiation with 1 g PEG for 30 min was consisted of small nanoparticles with the size of *ca.* 60 nm. The effects of ultrasonic irradiation and surfactant were investigated. The nanosized $BiVO_4$ exhibited excellent visible-light-driven photocatalytic efficiency for degrading organic dye, which was increased to nearly 12 times than that of the products prepared by traditional solid-state reaction. Besides decoloring, the reduction of chemical oxygen demand (COD) concentration was also observed in the degradation of organic dye, further demonstrating the photocatalytic performance of $BiVO_4$. After five recycles, the catalyst did not exhibit any significant loss of photocatalytic activity, confirming the photocatalyst is essentially stable. Close investigation revealed that the crystal size, BET surface area, and appropriate band gap of the as-prepared $BiVO_4$ could improve the photocatalytic activities.

1. Introduction

Visible-light-driven photocatalytic technology can help to alleviate the problems of modern societies by splitting water for hydrogen production as green energy and degrading toxic pollutants [1–4]. Photocatalysts such as TiO_2 has been intensively investigated [5–8]. But it can only be excited by ultraviolet radiation that occupies about 4% of the solar light. Visible-light-driven photocatalysts have received considerable attentions because visible-light ($400\,nm < \lambda < 800\,nm$) occupies the main part of the solar spectrum. Therefore, the development of efficient visible-light-driven photocatalysts is becoming attractive and a great deal of effort has been devoted into this research [9].

Bismuth vanadate ($BiVO_4$) has been recognized as a visible-light-driven photocatalyst for water splitting and pollutant decomposing under visible-light irradiation [10–18]. Various methods have been used to synthesize $BiVO_4$ crystallites, such as aqueous process [10,19–22], hydrothermal process [23–25], organic decomposition method [26], chemical bath deposition [27], solution combustion synthesis method [28], flame spray pyrolysis [29], and solid-state reaction (SSR) method [30]. Recently, our group has reported a sonochemical route to synthesize $BiVO_4$ photocatalyst with relative high photocatalytic activity [31]. Currently, sonochemical processing is found to be facile and efficient for the preparation of various nanostructures at room temperature and atmosphere pressure [32–34].

It is well known that the photocatalytic activity closely relates with the diameter size and surface area etc. of the photocatalyst [35,36]. Thus, the synthesis of nanosized $BiVO_4$ photocatalysts with high surface area is a subject of considerable research interest to improve photocatalytic efficiency. Very recently, the ordered mesoporous monoclinic scheelite $BiVO_4$ was fabricated by nanocasting, using mesoporous silica KIT-6 as the replica parent template [37]. Compared to conventional $BiVO_4$, the product exhibited good photocatalytic performance in the photochemical degradation of methylene blue under visible-light irradiation. It was also confirmed that the nanosized photocatalyst could assuredly improve the photocatalytic activity.

Herein, the nanosized $BiVO_4$ with high visible-light-induced photocatalytic activity was prepared via the ultrasonic-assisted method with polyethylene glycol (PEG) as the surfactant. It was found that ultrasonic irradiation and protective effect of PEG played an important role in the formation of the photocatalyst and the final photocatalytic performance. The photodegradation of Rhodamine B (RhB) was employed to evaluate the photocatalytic activities of $BiVO_4$ under visible-light ($\lambda > 420\,nm$) illumination. Reduction of chemical oxygen demand (COD) concentration was observed in the degradation of RhB, further confirming the photocatalytic performance of $BiVO_4$. It is demonstrated that the nanosized $BiVO_4$ exhibits relatively high performance in the visible-light-driven photocatalysis.

* Corresponding author. Tel.: +86 21 5241 5295; fax: +86 21 5241 3122.
E-mail address: wzwang@mail.sic.ac.cn (W. Wang).

0304-3894/$ – see front matter © 2009 Elsevier B.V. All rights reserved.
doi:10.1016/j.jhazmat.2009.07.017

2. Experimental

2.1. Synthesis

All the reagents used in our experiments were of analytical purity and were used as received from Shanghai Chemical Company. In a typical preparation, aqueous solutions of $Bi(NO_3)_3{\cdot}5H_2O$ and NH_4VO_3 in 1:1 molar ratio were mixed together. Subsequently, polyethylene glycol 20000, as surfactant, was added into the above solution. The pH value of the final suspension was adjusted to about 7 by $NH_3{\cdot}H_2O$. Then the mixture was stirred for 1 h at room temperature. Afterward, the mixture was exposed to high-intensity ultrasonic irradiation (6 mm diameter Ti-horn, 600 W, 20 kHz) at room temperature in ambient air. The yellow precipitates were centrifuged, washed with de-ionized water and absolute ethanol, and then dried at 60 °C in air for 10 h. The obtained powders were then calcined at 450 °C for 2 h to produce crystalline products. All PEG series samples were ultrasonic irradiated with 0–2 g PEG for 30 min, while all ultrasonic irradiation series samples were prepared with 1 g PEG for different minutes.

For comparison, the sample which was ultrasonic irradiated for 30 min without PEG (P1), the sample prepared with 1 g PEG but no ultrasonic irradiation (U1), and the sample without PEG and ultrasonic pretreatment (BVO) were also prepared while other steps were the same as above. Bulk $BiVO_4$ was synthesized via traditional solid-state reaction according to Ref. [30], named as SSR-BVO.

2.2. Characterization

The X-ray diffraction (XRD) patterns of the samples were measured on a D/MAX 2250 V diffractometer (Rigaku, Japan) using monochromatized Cu Kα ($\lambda = 0.15418$ nm) radiation under 40 kV and 100 mA and scanning over the range of $10^\circ \le 2\theta \le 70^\circ$. The crystal size was estimated from the Scherrer equation, $D = K\lambda/\mathrm{FWHM}\cos\theta$, where D is the crystal size, λ is the wavelength of the X-ray radiation and K usually is taken as 0.9, FWHM is the full width at half maximum in radian of the sample, and $2\theta = 28.6^\circ$. The morphologies and microstructures of as-prepared samples were analyzed by the scanning electron microscope (SEM) (JEOL JSM-6700F). UV–vis diffuse reflectance spectra of the samples were obtained on an UV–vis spectrophotometer (Hitachi U-3010) using $BaSO_4$ as the reference. Nitrogen adsorption–desorption measurements were conducted at 77.35 K on a Micromeritics Tristar 3000 analyzer after the samples were degassed at 200 °C for 6 h. The Brunauer–Emmett–Teller (BET) surface area was estimated using adsorption data. The photoluminescence (PL) spectra of the samples were recorded with a PerkinElmer LS55.

2.3. Photocatalytic test

Photocatalytic activities of the samples were evaluated by the photocatalytic decolorization of Rhodamine B under visible-light. A 500 W Xe lamp was used as the light source with a 420 nm cut-off filter to provide visible-light irradiation. In every experiment, 0.1 g of the photocatalyst was added into 100 mL RhB solution (10^{-5}–10^{-4} mol/L). Before illumination, the suspensions were magnetically stirred in the dark for 1 h to ensure the establishment of an adsorption–desorption equilibrium between the photocatalyst and RhB. Then the suspension was exposed to visible-light irradiation under magnetic stirring. At given time intervals, 3 mL suspension was sampled and centrifuged to remove the photocatalyst particles. Then, the UV–vis adsorption spectrum of the centrifugated solution was recorded using a Hitachi U-3010 UV–vis spectrophotometer. Chemical oxygen demand was estimated before and after the treatment using the $K_2Cr_2O_7$ oxidation method.

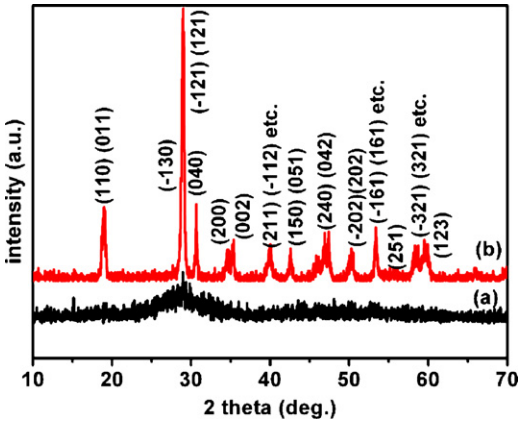

Fig. 1. XRD patterns of the calcined and uncalcined $BiVO_4$ samples: (a) uncalcined $BiVO_4$; (b) calcined $BiVO_4$.

Table 1
Size, band gap, BET surface area and degradation rate of $BiVO_4$ samples.

	Average size (nm)	BET (m^2/g)	Band gap (eV)	Degradation rate (%)
BVO	183	7.25	2.28	28
U1	645	9.09	2.24	42
P1	65	10.05	2.18	65
BVO-P-U	51	12.03	2.13	100

3. Results and discussion

3.1. Crystal structure

The phase and composition of the calcined sample, as well as the uncalcined sample were characterized by XRD, as shown in Fig. 1. The pattern of Fig. 1a indicates that the uncalcined $BiVO_4$ obtained after ultrasonic irradiation for 30 min with 1 g PEG is poorly crystallized. However, the calcination favors the formation of well-crystallized $BiVO_4$ comparatively, and the diffraction peaks of this sample (named as BVO-P-U) agree well with those of the pure monoclinic $BiVO_4$ according to the JCPDS No. 14-0688, as revealed in Fig. 1b. The cell constants calculated by the least squares refinement method are as follows: (a) 5.192 Å, (b) 11.701 Å, and (c) 5.091 Å, which are in agreement with the reported values (JCPDS No. 14-0688) [20,37]. The average crystallite size calculated from the strongest diffraction peak using the Scherrer equation is about 51 nm [37,38]. The average size of the other samples which were also calculated from the XRD (not given) were shown in Table 1.

3.2. Morphology and microstructure

The morphology and microstructure of the $BiVO_4$ samples were revealed by scanning electron microscopy (SEM). Fig. 2A is the SEM image of the BVO-P-U sample, showing that it is composed of well-separated nanoparticles with an average size of about 60 nm. The crystalline size is in good agreement with the value evaluated using Scherrer equation based on XRD patterns. To investigate the effect of ultrasonic irradiation and PEG on the morphology of $BiVO_4$ products, the SEM of P1, U1, and BVO samples were also shown in Fig. 2B, C, and D, respectively. As shown in Fig. 2B, most of the P1 particles which was ultrasonic irradiated for 30 min without PEG connected with each other and fusion was induced in the absence of PEG while the BVO-P-U were well dispersed. The morphology of U1 sample which was prepared with 1 g PEG but no ultrasonic irradiation was shown in Fig. 2C. The U1 sample is composed of rod-like particles with the average size of about 1000 nm. The morphology of the BVO sample without ultrasonic irradiation and PEG was revealed to be

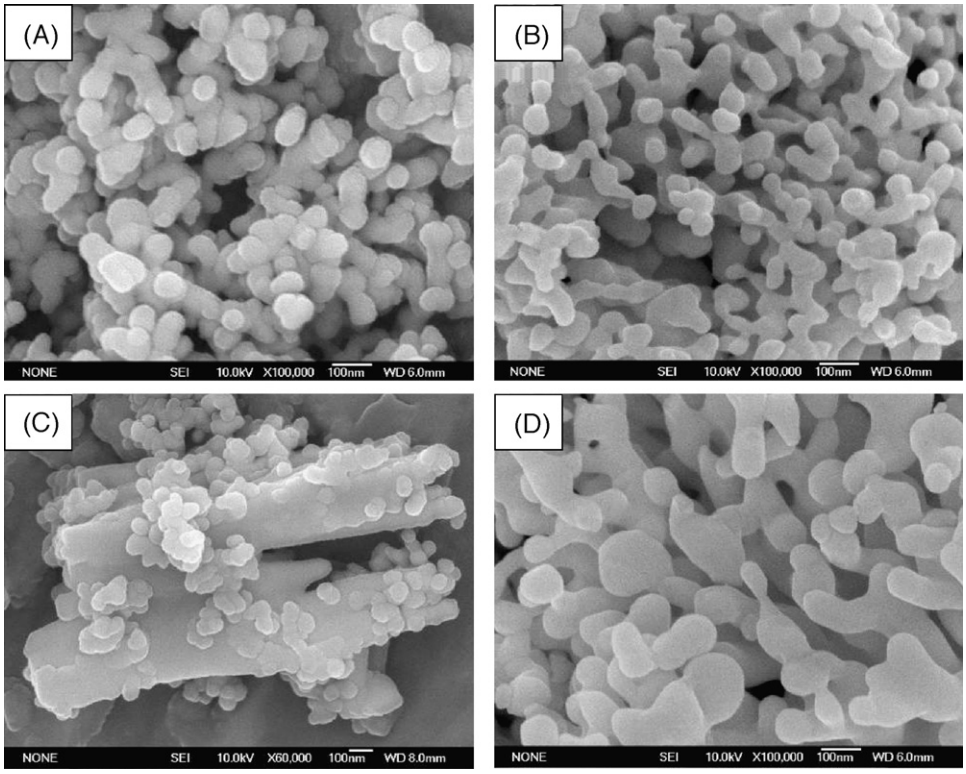

Fig. 2. SEM images of $BiVO_4$ samples: (A) the morphology of the BVO-P-U; (B) the morphology of P1; (C) the morphology of U1; (D) the morphology of BVO.

particles with the size ranging from 100 to 300 nm, as shown in Fig. 2D.

3.3. The effect of ultrasonic irradiation and surfactant

From the investigation of SEM, it is clearly that PEG and ultrasonic irradiation play a decisive part in controlling the size and morphology of $BiVO_4$ particles. In most cases, the surface passivation reagents, including surfactant molecules and polymers, are needed to prevent the nanoparticles from aggregation. The surface modification of these colloidal nanoparticles is very important to facilitate their application in biotechnology, catalysis, and nanocomposite [39]. Here, the use of high-molecular-weight PEG-20000 aids in the formation of nanosized and well-separated $BiVO_4$ particles with an approximate size of 60 nm. PEG is a kind of nonionic surfactant which is obtained by the polyesterification reaction between ethylene alcohol and epoxy ethane, and has the following structure that is characterized by hydroxyl groups at either end of the molecule:

$HO–(CH_2CH_2O)_nCH_2CH_2–OH$

where n is the polymerization number. It is a linear or branched, neutral polyether available in a variety of molecular weights and is soluble in water and most organic solvents. In which oxygen atoms is hydrophilic and the group of $–CH_2–CH_2–$ is hydrophobic. The ether oxygen on the fundamental chain is prone to adsorb positive ions and can interact with metal ions [40] in the solution to form chain-like coordination complexes. The possible reactions could be proposed as follows:

$$Bi(NO_3)_3 \rightarrow Bi^{3+} + 3NO_3^- \quad (a)$$

$$NH_4VO_3 \rightarrow NH_4^+ + VO_3^- \quad (b)$$

$$Bi^{3+} + VO_3^- + H_2O \rightarrow BiVO_4 + 2H^+ \quad (c)$$

$$Bi^{3+} + VO_3^- \xrightarrow{PEG} PEG - Bi^{3+}\cdots VO_3^- \quad (d)$$

$$PEG - Bi^{3+}\cdots VO_3^- + H_2O \xrightarrow{US} BiVO_4 + PEG + 2H^+ \quad (e)$$

The possible formation of the as-prepared $BiVO_4$ samples and the effect of PEG and ultrasound were depicted in Scheme 1. As shown in Eq. (a), Bi^{3+} will produce when $Bi(NO_3)_3$ dissolve in acid solution. And VO_3^- will produce when NH_4VO_3 dissolve in water (Eq. (b)). When these two solutions are mixed, a yellow precipitate of amorphous $BiVO_4$ will produce immediately (Eq. (c)). Because this precipitation process carries out naturally, during the calcination the intrinsic nucleation and anisotropic growth of the $BiVO_4$ is dominant in determining the microstructure of the product, thus big particles will be obtained (Scheme 1, BVO). However, when PEG was added in the solution, Bi^{3+} can coordinate with PEG (Eq. (d)), which results in the decrease of Bi^{3+} concentration. Therefore, after VO_3^- solution was added, the reaction between Bi^{3+} and VO_3^- is partly inhibited, which may result in an intermediate species in definite growth time but no yellow precipitate $BiVO_4$ produced immediately. Moreover, due to the chain-like coordination complexes, the $BiVO_4$ may aggregate and crystallize into big rod-like particles during the calcination (Scheme 1, U1). On the other hand, besides the morphology was tuned due to the coordination effect of PEG, the protective effect is another function during

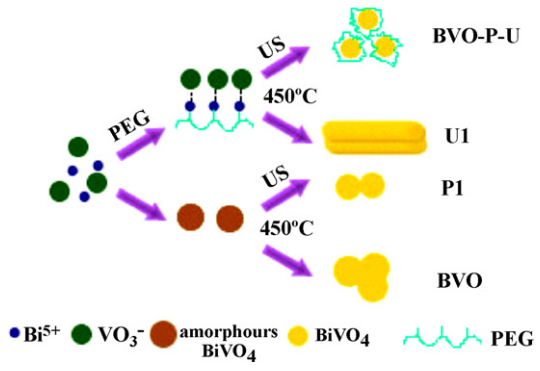

Scheme 1. The formation mechanism of the as-prepared samples.

the ultrasonic irradiation. The sonochemical techniques have been recently developed for the fast synthesis of nanosized functional inorganic materials. It is expected that sonochemical approach may create inorganic materials with smaller crystal size and higher surface area. When a suitable precursor is irradiated with high-intensity ultrasound, acoustic cavitations (the formation, growth, and implosive collapse of the bubbles) can provide very high temperatures (>5000 K), high pressures (>20 MPa), and cooling rates in excess of 109 K/s [41]. Under the ultrasonic irradiation, the complex will gradually decompose to release Bi^{3+} slowly, followed by the reaction with VO_3^-, as shown in Eq. (e). The amorphous $BiVO_4$ sediment was generated under this circumstance. Moreover, PEG may adsorb on the surface of amorphous $BiVO_4$ and act as the template and the protective agent so as to favor the formation of smaller granular grains during ultrasonic irradiation. As a result, after calcination the nanosized and well-separated $BiVO_4$ was obtained (Scheme 1, BVO-P-U) [42]. In the absence of PEG, the amorphous $BiVO_4$ with big sizes may become smaller under the condition of ultrasound, but most of the particles may connect with each other and fusion was induced due to the lack of PEG protective effect (Scheme 1, P1).

The electronic structure of $BiVO_4$ has been reported based on the DFT calculations [43]. It has been reported that the valence band of the $BiVO_4$ is formed by the hybrid orbitals of Bi 6s and O 2p and the conduction band of V 3d, so the band gap becomes narrower and the considerable absorption extends up to the visible region. This special electronic structure makes the valence band largely dispersed, and facilitates the mobility of photo-excited holes to the surface of the crystal and thus is beneficial to photocatalytic oxidation of organic pollutants.

3.4. UV–vis diffuse reflectance spectra and band gap

The optical absorption property of a semiconductor, which is relevant to the electronic structure feature, is recognized as the key factor in determining its photocatalytic activity [44]. The optical properties of the $BiVO_4$ samples were measured using UV–vis spectroscopy. Fig. 3 shows the diffuse reflectance spectra of the $BiVO_4$ samples (a: BVO; b: U1; c: P1; d: BVO-P-U). The samples showed strong absorption in visible-light region in addition to that in the UV light region, which implying the possibility of photocatalytic activity over these materials under visible-light irradiation. Based on the equation $ah\nu = A(h\nu - E_g)^{n/2}$ [45], the band gaps of the samples were estimated to be 2.28, 2.24, 2.18, and 2.13 eV from the onset of the absorption edges, corresponding to the BVO, U1, P1, BVO-P-U sample, respectively, as shown in Table 1. Such differences may be attributed to the changes of crystallite phase and the size of coupled oxides, defects, and so on [31,46,47]. With the presence of ultrasonic irradiation and PEG, the samples show a stronger absorption in the visible range and shift in the band gap transition. The shift may be ascribed to the size effect and crystal defects.

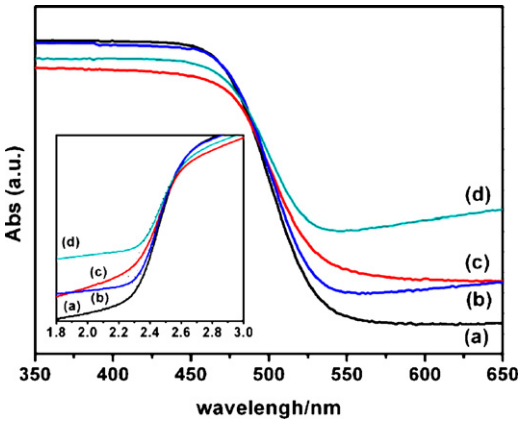

Fig. 3. The UV–vis diffuse reflectance spectra of the $BiVO_4$ samples: (a) BVO; (b) U1; (c) P1; (d) BVO-P-U. The inset shows the relationship between $(\alpha h\nu)^2$ and photon energy.

3.5. Photocatalytic activities

The photocatalytic activities of $BiVO_4$ were evaluated by the degradation of RhB dye in water under visible-light irradiation ($\lambda > 420$ nm) using a 500 W Xe lamp. The temporal UV–vis spectral changes of RhB aqueous solution during the photocatalytic degradation reactions are showed in Fig. 4A. As seen in Fig. 4A, when the RhB solution was irradiated with visible-light ($\lambda > 420$ nm) in the presence of BVO-P-U sample, about 95% of RhB was degraded after being irradiated for 30 min and the spectral maximum shifted from 552 to 500 nm. The color of the suspension changed gradually from pink to light green. Further irradiation to 40 min caused the decrease of the absorption band at 500 nm, and the color of the suspension changed sequentially colorless. Fig. 4B showed the efficiencies of the photocatalytic degradation under visible-light irradiation, C was the absorption of RhB at the wavelength of 552 nm and C_0 was the absorption after the adsorption equilibrium on $BiVO_4$ samples before irradiation. Blank test (RhB without any catalyst) under visible-light exhibited little photolysis. The photodegradation efficiency was only 4% after 40 min, which demonstrates that the degradation of RhB is extremely slow without a photocatalyst under visible-light illumination. The decrease of RhB with the nanosized $BiVO_4$ in the dark condition for 40 min was similar to that of the blank test, which demonstrated that the absorption of RhB on the as-prepared $BiVO_4$ was limited after the adsorption–desorption equilibrium reached. With the BVO-P-

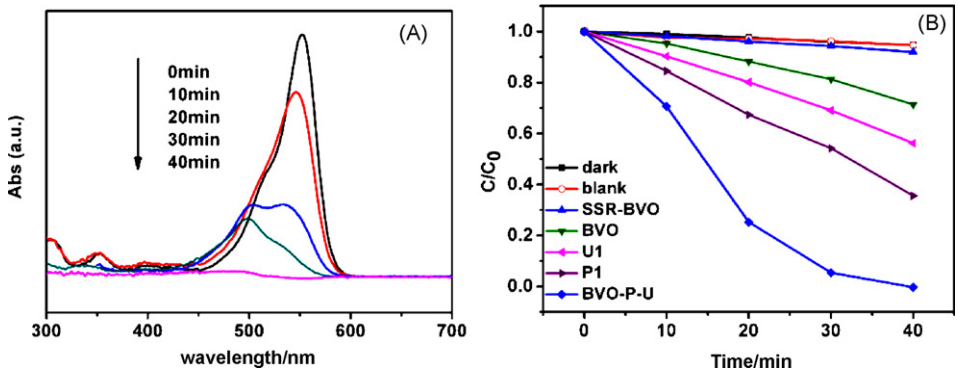

Fig. 4. Photocatalytic degradation of RhB using $BiVO_4$ samples: (A) the changes of temporal UV–vis spectral of RhB aqueous solution; (B) comparison of BVO-P-U, P1, U1, BVO, SSR-BVO, and blank tests.

U sample which was ultrasonic irradiated with 1 g PEG for 30 min, the photodegradation efficiency of RhB reaches nearly 100% after 40 min irradiation only. However, the photocatalytic activities of P1, U1, and BVO sample were only 65%, 42%, and 28% after irradiating for 40 min, respectively, as shown in Table 1. The experiments also showed that the photocatalytic activity of the BVO-P-U sample was much higher than that of the SSR-BVO sample (12 times), which demonstrated that the surfactant and ultrasonic irradiation played a key role in enhancing photocatalytic activity of $BiVO_4$.

In order to measure the pollution strength of the dye, chemical oxygen demand of the dye solutions was assessed before and after its removal during photocatalytic degradation. The chemical oxygen demand test is widely used as an effective technique to measure the organic strength of wastewater. The test allows the measurement of waste in terms of the total quantity of oxygen required for the oxidation of organic matter to CO_2 and water [48]. If the dye was not degraded completely, the residual organic molecules could be oxidized by $K_2Cr_2O_7$, thus the oxygen demanded could be more. In other words, the COD value of the cracked dye would be higher than that of the completely mineralized dye. As the reduction of COD reflects the extent of degradation or mineralization of an organic species along with the decolorization, the percentage change of COD in the photodegradation of RhB with high concentration (10^{-4} M) was studied as a function of longer irradiation time (3.5 h) of visible-light so as to demonstrate the ability of photodegradation clearly of the BVO-P-U photocatalyst, as shown in Fig. 5. A significant decrease in the COD values of the Rhodamine B solution was observed. The initial COD concentration of the RhB solution (10^{-4} mol/L) is 248.6 mg/L, and the *T*% (measured at 500 nm) is 1.2%. After visible-light irradiation for 3.5 h, the COD concentration decreased to 67.76 mg/L, and the *T*% at 500 nm reached 95%. The reduction of COD (72.7%) and the increase of the *T*% further confirm that RhB was truly photodegraded by nanosized $BiVO_4$.

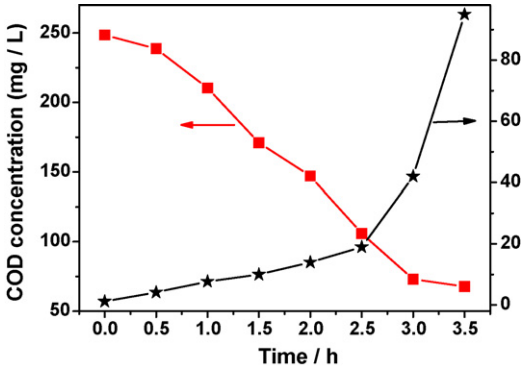

Fig. 5. Variation of COD and transmittance of RhB (10^{-4} M) aqueous solutions with irradiation time (catalyst, 0.1 g). Inset: UV–vis spectral changes of the RhB (10^{-4} M) aqueous solution as a function of irradiation time.

To study the influence of surfactant and ultrasonic irradiation on the photocatalytic activity, the degradation of RhB by using PEG series of $BiVO_4$ samples (P1: 0 g; P2: 0.5 g; BVO-P-U: 1 g; P3: 2 g) and ultrasonic irradiation series of $BiVO_4$ samples (U1: 0 min; U2: 10 min; BVO-P-U: 30 min; U3: 60 min) were shown in Fig. 6A and B. P1 sample exhibited worst photocatalytic activity without PEG. With the increasing concentration of PEG, the photocatalytic activities of the $BiVO_4$ samples enhanced. The PEG suppresses the agglomeration of the $BiVO_4$ particles and induces the formation of nanosized particles. However, with the increase of PEG concentration further, the function of protective effect under the ultrasonication faded out. On the other hand, the result of aggre-

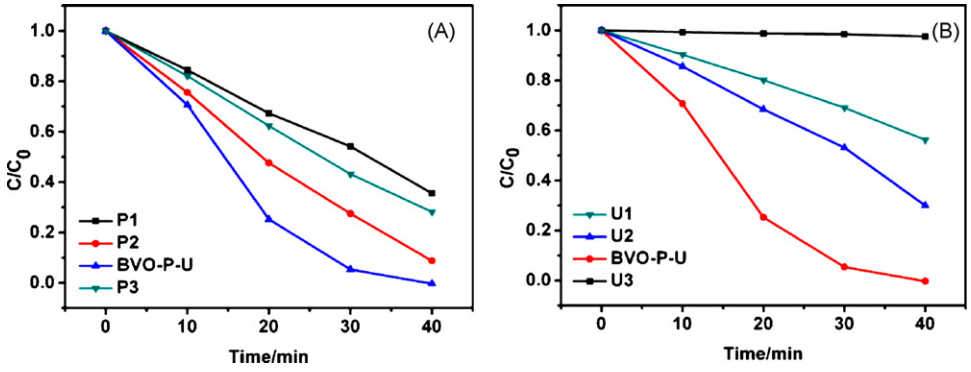

Fig. 6. (A) The photocatalytic degradation of RhB using PEG series for ultrasonic irradiating 30 min; (B) the photocatalytic degradation of RhB using ultrasonic irradiation series with 1 g PEG.

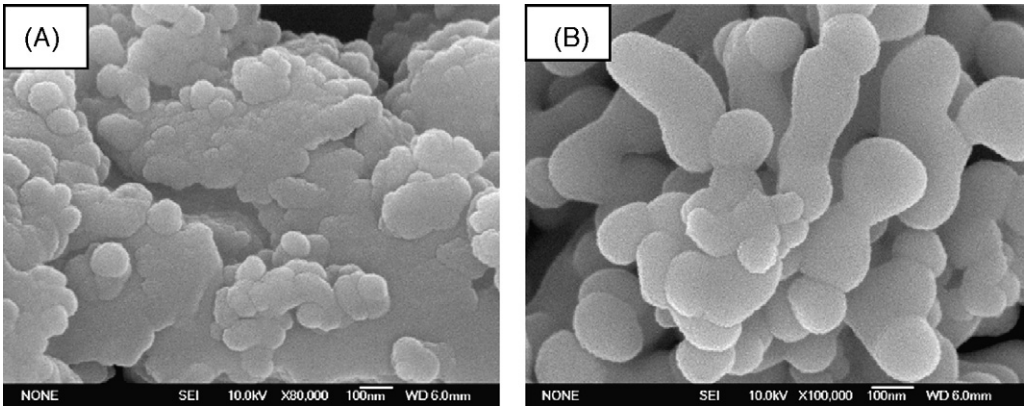

Fig. 7. The SEM images of P3 sample (A) and U3 sample (B).

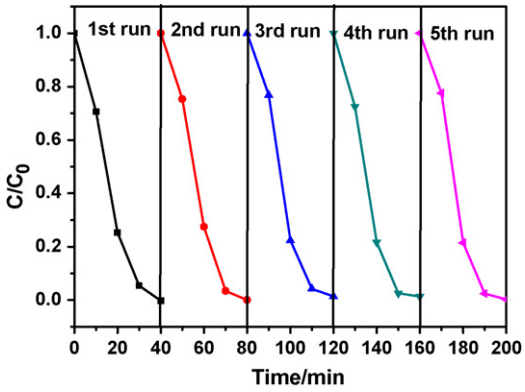

Fig. 8. Cycling runs in the photocatalytic degradation of RhB in the presence of nanosized $BiVO_4$ under visible-light.

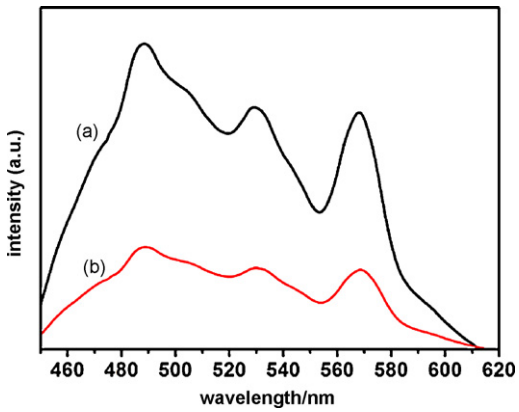

Fig. 9. The room temperature photoluminescence (PL) spectrum of SSR-BVO (a), and BVO-P-U (b) (λ_{Ex} = 375 nm).

gation which may enlarge the particle size was produced. The SEM image demonstrated that the particles (about 100 nm) connected with each other and agglomeration was induced due to the excess of PEG (Fig. 7A). Therefore, the photocatalytic activity of sample decreased when more PEG was added (Fig. 6A). As shown in Fig. 6B, the photodegradation efficiency was enhanced with the increasing time of ultrasonic irradiation. Whereas, the photocatalytic activity was decreased sharply when the time was 1 h, which may be resulted from the particle growth promoted by ultrasonic irradiation energy (Fig. 7B). Additionally, the crystal defects which work as recombination sites of photogenerated electrons and hole may be formed at the instantly high temperature during ultrasonic irradiation [10]. Both of the increased size and crystal defects could decrease the photocatalytic activity.

To confirm the stability of the high photocatalytic performance of the nanosized $BiVO_4$, the circulating runs in the photocatalytic degradation of RhB in the presence of $BiVO_4$ under visible-light ($\lambda > 420$ nm) were checked (Fig. 8). After five recycles for the photodegradation of RhB, the catalyst did not exhibit any significant loss of activity. It indicates that the nanosized $BiVO_4$ has high stability and does not photocorrode during the photocatalytic oxidation of the model pollutant molecules, which is especially important for its application.

The enhanced photocatalytic activity of nanosized $BiVO_4$ is due to its physicochemical properties such as crystal size, BET surface area, and appropriate band gap. The photocatalytic behavior is closely related to the efficiency of the photogenerated electron–hole separation. For randomly generated charge carriers the average diffusion time from the bulk to the surface is given by $\tau = r^2/\pi^2 D$, where r is the grain radius and D is the diffusion coefficient of the carrier [49]. If the grain radius decreases, it will reduce the recombination opportunities of the photogenerated electron–hole pairs which could diffuse effectively to the surface to generate oxidative species. PL emission spectra are useful in determining the efficiency of charge carrier trapping, migration and transfer, and helpful in understanding the fate of electron–hole pairs in semiconductor particles, since it mainly results from the recombination of excited electrons and holes. A low PL intensity implies a low recombination rate of the electron–hole under light irradiation [50]. Fig. 9 shows the comparison of PL spectra of SSR-BVO sample and BVO-P-U sample when the excitation wavelength was 375 nm. It was found that the PL emission spectra of two photocatalysts showed the main peaks at similar positions but with different intensities. The PL intensity of BVO-P-U sample is lower than that of SSR-BVO sample, which clearly indicates that the recombination of the hole formed in the O 2p band and the electron in the V 3d band is greatly inhibited [12]. The size of the BVO-P-U sample is only 60 nm, which could be beneficial for promoting the efficiency of the electron–hole separation, transferring to the surface, and acting with the organic molecules. Meanwhile, the Brunauer–Emmett–Teller has been used to characterize the surface area since the photocatalytic activities are related to the surface area of photocatalysts, as shown in Table 1. The BET surface area of BVO-P-U sample was estimated to be *ca.* 12.03 m^2/g, which was much higher than of the reference SSR-$BiVO_4$ sample of *ca.* 0.26 m^2/g. A large surface area not only supplies more active sites for the degradation reaction of organic compounds but also effectively promotes the separation efficiency of the electron–hole pairs, resulting in a higher activity of the photocatalytic reaction [37]. Moreover, the band gap of $BiVO_4$ may also contribute to its photocatalytic activity. The optical absorption property of a semiconductor, which is relevant to the electronic structure feature, is recognized as the key factor in determining its photocatalytic activity. As a direct electron transition semiconductor, the monoclinic $BiVO_4$ crystal is excited by the incident photons with energy equal to or greater than their band energy level. The electrons receive energy from the photons and are thus promoted from the valence band to the conduction band, if the energy gained is higher than the band gap energy level. Electrons and holes that migrate to the surface of the semiconductor without recombination can respectively reduce or oxidize the reactants adsorbed by the semiconductor. All these $BiVO_4$ samples have suitable band gap (Fig. 3) which can be excited by visible-light for photocatalytic decomposition of organic contaminants. With the increase of the photoabsorption, more photogenerated electron–hole pairs could be produced under visible-light thus the photocatalytic activities were enhanced. The BVO-P-U sample exhibited the highest photocatalytic activity than other samples due to its smallest particle size and suitable band gap. Additionally, the catalyst U1 with relatively bigger particle size exhibited higher photocatalytic activity than BVO due to the appropriate band gap which had the longer wavelength of absorption, although other factors may contribute to its photocatalytic activities and co-relate with each other.

4. Conclusions

In summary, the nanosized $BiVO_4$ (60 nm) was successfully prepared utilizing polyethylene glycol as the surfactant via the ultrasonic-assisted method. It was found that ultrasonic irradiation and surfactant play an important role in the formation of nanosized $BiVO_4$. Compared with the samples prepared by solid-state reaction, the $BiVO_4$ sample exhibited higher photocatalytic activity (nearly 12 times) in the degradation of RhB under visible-light irradiation. Furthermore, the reduction of COD concentration also demonstrated the photocatalytic performance of $BiVO_4$. The

sample possessed a large surface area, an appropriate band gap, and a small crystal size, resulting in excellent visible-light photocatalytic activity. This work not only provides an example of size-dependent photocatalytic properties but also opens new possibilities to provide some insight into the design of new high activity photocatalysts for degrading organic pollutants and other applications.

Acknowledgements

We acknowledge the financial support from the National Natural Science Foundation of China (Nos. 50672117 and 50732004) and the Nanotechnology Programs of Science and Technology Commission of Shanghai (0852nm00500).

References

[1] M.R. Hoffmann, S.T. Martin, W. Choi, D.W. Bahnemann, Environmental applications of semiconductor photocatalysis, Chem. Rev. 95 (1995) 69–96.
[2] X.C. Wang, J.C. Yu, Y.L. Chen, L. Wu, X.Z. Fu, ZrO_2-modified mesoporous nanocrystalline $TiO_{2-x}N_x$ as efficient visible light photocatalysts, Environ. Sci. Technol. 40 (2006) 2369–2374.
[3] E. Bizani, K. Fytianos, I. Poulios, V. Tsiridis, Photocatalytic decolorization and degradation of dye solutions and wastewaters in the presence of titanium dioxide, J. Hazard. Mater. 136 (2006) 85–94.
[4] M. Asilturk, F. Sayilkan, S. Erdemoglu, M. Akarsu, H. Sayilkan, M. Erdemoglu, E. Arpac, Characterization of the hydrothermally synthesized nano-TiO_2 crystallite and the photocatalytic degradation of Rhodamine B, J. Hazard. Mater. 129 (2006) 164–170.
[5] G.S. Li, J.C. Yu, J. Zhu, Y. Cao, Hierarchical mesoporous grape-like titania with superior recyclability and photoactivity, Microporous Mesoporous Mater. 106 (2007) 278–283.
[6] L.Q. Jing, X.J. Sun, J. Shang, W.M. Cai, Z.L. Xu, Y.G. Du, H.G. Fu, Review of surface photovoltage spectra of nano-sized semiconductor and its applications in heterogeneous photocatalysis, Solar Energy Mater. Solar Cells 79 (2003) 133–151.
[7] J. Yu, L. Zhang, Z. Zheng, J. Zhao, Synthesis and characterization of phosphated mesoporous titanium dioxide with high photocatalytic activity, Chem. Mater. 15 (2003) 2280–2286.
[8] W.Y. Teoh, R. Amal, L. Madler, S.E. Pratsinis, Flame sprayed visible light-active Fe-TiO_2 for photomineralisation of oxalic acid, Catal. Today 120 (2007) 203–213.
[9] I. Tsuji, H. Kato, A. Kudo, Visible-light-induced H_2 evolution from an aqueous solution containing sulfide and sulfite over ZnS-$CuInS_2$-$AgInS_2$ solid solution photocatalyst, Angew. Chem. Int. Ed. 44 (2005) 3565–3568.
[10] A. Kudo, K. Omori, H. Kato, A novel aqueous process for preparation of crystal form-controlled and highly crystalline $BiVO_4$ powder from layered vanadates at room temperature and its photocatalytic and photophysical properties, J. Am. Chem. Soc. 121 (1999) 11459–11467.
[11] S. Kohtani, M. Koshiko, A. Kudo, K. Tokumura, Y. Ishigaki, A. Toriba, K. Hayakawa, R. Nakagaki, Photodegradation of 4-alkylphenols using $BiVO_4$ photocatalyst under irradiation with visible light from a solar simulator, Appl. Catal. B: Environ. 46 (2003) 573–586.
[12] M. Long, W.M. Cai, J. Cai, B.X. Zhou, X.Y. Chai, Y.H. Wu, Efficient photocatalytic degradation of phenol over Co_3O_4/$BiVO_4$ composite under visible light irradiation, J. Phys. Chem. B 110 (2006) 20211–20216.
[13] L. Zhang, D.R. Chen, X.L. Jiao, Monoclinic structured $BiVO_4$ nanosheets: hydrothermal preparation, formation mechanism, and coloristic and photocatalytic properties, J. Phys. Chem. B 110 (2006) 2668–2673.
[14] K. Sayama, A. Nomura, T. Arai, T. Sugita, R. Abe, M. Yanagida, T. Oi, Y. Iwasaki, Y. Abe, H. Sugihara, Photoelectrochemical decomposition of water into H_2 and O_2 on porous $BiVO_4$ thin-film electrodes under visible light and significant effect of Ag ion treatment, J. Phys. Chem. B 110 (2006) 11352–11360.
[15] F. Rullens, A. Laschewsky, M. Devillers, Bulk and thin films of bismuth vanadates prepared from hybrid materials made from an organic polymer and inorganic salts, Chem. Mater. 18 (2006) 771–777.
[16] L. Ge, Novel Pd/$BiVO_4$ composite photocatalysts for efficient degradation of methyl orange under visible light irradiation, Mater. Chem. Phys. 107 (2008) 465–470.
[17] D.N. Ke, T.Y. Peng, L. Ma, P. Cai, P. Jiang, Photocatalytic water splitting for O_2 production under visible-light irradiation on $BiVO_4$ nanoparticles in different sacrificial reagent solutions, Appl. Catal. A: Gen. 350 (2008) 111–117.
[18] P. Chatchai, Y. Murakami, S.Y. Kishioka, A.Y. Nosaka, Y. Nosaka, Efficient photocatalytic activity of water oxidation over WO_3/$BiVO_4$ composite under visible light irradiation, Electrochim. Acta 54 (2009) 1147–1152.
[19] B.P. Xie, H.X. Zhang, P.X. Cai, R.L. Qiu, Y. Xiong, Simultaneous photocatalytic reduction of Cr(VI) and oxidation of phenol over monoclinic $BiVO_4$ under visible light irradiation, Chemosphere 63 (2006) 956–963.
[20] L. Zhou, W.Z. Wang, L.S. Zhang, H.L. Xu, W. Zhu, Single-crystalline $BiVO_4$ microtubes with square cross-sections: microstructure, growth mechanism, and photocatalytic property, J. Phys. Chem. C 111 (2007) 13659–13664.
[21] L. Zhou, W.Z. Wang, H.L. Xu, Controllable synthesis of 3D well-defined $BiVO_4$ mesocrystals via a facile additive-free aqueous strategy, Cryst. Growth Des. 8 (2008) 728–733.
[22] H.M. Luo, H.A. Mueller, M.T. McCleskey, K.A. Burrell, E. Bauer, Q.X. Jia, Structural and photoelectrochemical properties of $BiVO_4$ thin films, J. Phys. Chem. C 112 (2008) 6099–6102.
[23] X. Zhang, Z.H. Ai, F.L. Jia, L.Z. Zhang, X.X. Fan, Z.G. Zou, Selective synthesis and visible-light photocatalytic activities of $BiVO_4$ with different crystalline phases, Mater. Chem. Phys. 103 (2007) 162–168.
[24] J.B. Liu, H. Wang, S. Wang, H. Yan, Hydrothermal preparation of $BiVO_4$ powders, Mater. Sci. Eng. B 104 (2003) 36–39.
[25] Y. Zhao, Y. Xie, X. Zhu, S. Yan, S.X. Wang, Surfactant-free synthesis of hyperbranched monoclinic bismuth vanadate and its applications in photocatalysis, gas sensing, and lithium-ion batteries, Chem. Eur. J. 14 (2008) 1601–1606.
[26] K. Sayama, A. Nomura, Z. Zou, R. Abe, Y. Abe, H. Arakawa, Photoelectrochemical decomposition of water on nanocrystalline $BiVO_4$ film electrodes under visible light, Chem. Commun. 23 (2003), 2908–1909.
[27] M.C. Neves, T. Trindade, Chemical bath deposition of $BiVO_4$, Thin Solid Films 406 (2002) 93–97.
[28] H.Q. Jiang, H. Endo, H. Natori, M. Nagai, K. Kobayashi, Fabrication and photoactivities of spherical-shaped $BiVO_4$ photocatalysts through solution combustion synthesis method, J. Eur. Ceram. Soc. 28 (2008) 2955–2962.
[29] R. Strobel, H.J. Metz, S.E. Pratsinis, Brilliant yellow, transparent pure, and SiO_2-coated $BiVO_4$ nanoparticles made in flames, Chem. Mater. 20 (2008) 6346–6351.
[30] M. Gotic, S. Music, M. Ivanda, M. Soufek, S. Popovic, Synthesis and characterization of bismuth(III) vanadate, J. Mol. Struct. 744 (2005) 535–540.
[31] L. Zhou, W.Z. Wang, S.W. Liu, L.S. Zhang, H.L. Xu, W. Zhu, A sonochemical route to visible-light-driven high-activity $BiVO_4$ photocatalyst, J. Mol. Catal. A: Chem. 252 (2006) 120–124.
[32] M.M. Mdleleni, T. Hyeon, K.S. Suslick, Sonochemical synthesis of nanostructured molybdenum sulfide, J. Am. Chem. Soc. 120 (1998) 6189–6190.
[33] N.A. Dhas, K.S. Suslick, Sonochemical preparation of hollow nanospheres and hollow nanocrystals, J. Am. Chem. Soc. 127 (2005) 2368–2369.
[34] J.G. Yu, M.H. Zhou, B. Cheng, H.G. Yu, X.J. Zhao, Ultrasonic preparation of mesoporous titanium dioxide nanocrystalline photocatalysts and evaluation of photocatalytic activity, J. Mol. Catal. A 227 (2005) 75–80.
[35] L. Zhang, J. Lin, Z. Chen, Y. Tang, Y. Yu, Preparation of Fenton reagent with H_2O_2 generated by solar light-illuminated nano-Cu_2O/MWNTs composites, Appl. Catal. A: Gen. 299 (2006) 292–297.
[36] M. Shang, W.Z. Wang, S.M. Sun, L. Zhou, L. Zhang, Bi_2WO_6 nanocrystals with high photocatalytic activities under visible light, J. Phys. Chem. C 112 (2008) 10407–10411.
[37] G.S. Li, D.Q. Zhang, J.C. Yu, Ordered mesoporous $BiVO_4$ through nanocasting: a superior visible light-driven photocatalyst, Chem. Mater. 20 (2008) 3983–3992.
[38] A. Enesca, A. Duta, J. Schoonman, Study of photoactivity of tungsten trioxide (WO_3) for water splitting, Thin Solid Films 515 (2007) 6371–6374.
[39] V.F. Puntes, K.M. Krishnan, A.P. Alivisatos, Colloidal nanocrystal shape and size control: the case of cobalt, Science 291 (2001) 2115–2117.
[40] T. Okada, Complexation of poly(oxyethylene) in analytical chemistry: a review, Analyst 118 (1993) 959–971.
[41] K.S. Suslick, S.B. Choe, A.A. Cichowlas, M.W. Grinstaff, Sonochemical synthesis of amorphous iron, Nature 353 (1991) 414–416.
[42] N. Zhang, W.B. Bu, Y.P. Xu, D.Y. Jiang, J.L. Shi, Surfactant-assisted growth of novel $La_2(MoO_4)_3$ dendritic nanostructures via facile hydrothermal processes, J. Nanosci. Nanotechnol. 8 (2008) 1468–1472.
[43] M. Oshikiri, M. Boero, J. Ye, Z. Zou, G. Kido, Electronic structures of promising photocatalysts $InMO_4$ (M = V, Nb, Ta) and $BiVO_4$ for water decomposition in the visible wavelength region, J. Chem. Phys. 117 (2002) 7313.
[44] J. Tang, Z. Zou, J. Ye, Efficient photocatalytic decomposition of organic contaminants over $CaBi_2O_4$ under visible-light irradiation, Angew Chem. Int. Ed. 43 (2004) 4463–4466.
[45] M.A. Butler, Photoelectrolysis and physical properties of the semiconducting electrode WO_3, J. Appl. Phys. 48 (1977) 1914–1920.
[46] M.L. Zhang, T.C. An, X.H. Hu, C. Wang, G.Y. Sheng, J.M. Fu, Preparation and photocatalytic properties of a nanometer ZnO-SnO_2 coupled oxide, Appl. Catal. A: Gen. 260 (2004) 215–220.
[47] J.G. Yu, J.F. Xiong, B. Cheng, Y. Yu, J.B. Wang, Hydrothermal preparation and visible-light photocatalytic activity of Bi_2WO_6 powders, J. Solid State Chem. 178 (2005) 1968–1972.
[48] R. Jain, M. Mathur, S. Sikarwar, A. Mittal, Removal of the hazardous dye rhodamine B through photocatalytic and adsorption treatments, J. Environ. Manage. 85 (2007) 956–964.
[49] A. Hagfeldt, M. Gratzel, Light-induced redox reactions in nanocrystalline systems, Chem. Rev. 95 (1995) 49–68.
[50] K. Fujihara, S. Izumi, T. Ohno, M. Matsumura, Time-resolved photoluminescence of particulate TiO_2 photocatalysts suspended in aqueous solutions, J. Photochem. Photobiol. A: Chem. 132 (2000) 99–104.